electronic reprint

Acta Crystallographica Section D
Biological Crystallography
ISSN 0907-4449
Editors: **E. N. Baker and Z. Dauter**

Structure of the *Yersinia pestis* type III secretion chaperone SycH in complex with a stable fragment of YscM2

Jason Phan, Joseph E. Tropea and David S. Waugh

Acta Crystallographica Section D
Biological Crystallography
ISSN 0907-4449

Structure of the *Yersinia pestis* type III secretion chaperone SycH in complex with a stable fragment of YscM2

Jason Phan, Joseph E. Tropea and David S. Waugh*

Protein Engineering Section, Macromolecular Crystallography Laboratory, Center for Cancer Research, National Cancer Institute at Frederick, PO Box B, Frederick, MD 21702, USA

Correspondence e-mail: waughd@ncifcrf.gov

Received 23 June 2004
Accepted 16 July 2004

PDB Reference: *Y. pestis* SycH in complex with a fragment of YscM2, 1ttw, r1ttwsf.

Pathogenic *Yersinia* species use a type III secretion system to inject cytotoxic effector proteins directly into the cytosol of mammalian cells, where they neutralize the innate immune response by interfering with the signal-transduction pathways that control phagocytosis and inflammation. To be exported efficiently, some effectors must transiently associate with cognate cytoplasmic secretion chaperones. SycH is the chaperone for YopH, a potent eukaryotic-like protein tyrosine phosphatase that is essential for virulence. SycH also binds two negative regulators of type III secretion, YscM1 and YscM2, both of which share significant sequence homology with the chaperone-binding domain of YopH. Here, the structure of a complex between SycH and a stable fragment of YscM2 that was designed on the basis of limited proteolysis experiments is presented. The overall fold of SycH is very similar to the structures of other homodimeric secretion chaperones that have been determined to date. YscM2 wraps around SycH in an extended fashion, with some secondary but no tertiary structure, assuming a conformation distinct from the globular fold that it is predicted to adopt in the absence of SycH.

1. Introduction

Like many Gram-negative bacterial pathogens of plants and animals, *Yersinia pestis*, the causative agent of plague, utilizes a type III secretion system (TTSS) to inject cytotoxic effector proteins directly into the cytosol of mammalian cells (reviewed by Cornelis, 2002). The anti-host activities of these effectors enable the bacterium to subvert the innate immune response of the infected organism. Four of the six *Yersinia* effectors (YopE, YopH, YpkA and YopT) inhibit phagocytosis by altering actin-cytoskeleton dynamics. YopJ suppresses the inflammatory response by interfering with signaling through the MAP kinase and NFκB pathways. The role of the sixth effector, YopM, remains obscure.

The primary signals that selectively target the effectors for type III secretion map to their N-termini, within the first 10–20 codons (Sory *et al.*, 1995; Schesser *et al.*, 1996; Boland *et al.*, 1996). However, they do not resemble the classic signal peptides associated with *sec*-dependent (type II) secretion and no residues are cleaved during transit. Although there is still some controversy as to whether the secretion signals are encoded within the amino-acid sequence of the effectors or in their mRNAs (Ramamurthi & Schneewind, 2003), a preponderance of evidence favors the former hypothesis. It has been suggested that a disordered amphipathic amino-terminus may be sufficient to target proteins for type III secretion (Lloyd *et al.*, 2002).

All effectors rely upon a primary N-terminal secretion signal for efficient export *via* the type III pathway. Addition-

ally, some of them must form transient complexes with cognate secretion chaperones (Sycs) in order to be secreted efficiently. The role of the secretion chaperones is not entirely clear, since not all effectors require them (Trulzsch *et al.*, 2003). Several proposals have been put forth: (i) that they act to maintain their cognate effectors in a translocation-competent (perhaps partially unfolded) state (Stebbins & Galan, 2001), (ii) that they afford some protection from intracellular proteolysis and/or prevent premature interactions between effectors and other components of the TTSS in the bacterial cytosol (Wattiau *et al.*, 1996) and (iii) that they establish a hierarchy of secretion for the various effectors, thereby controlling the timing of their delivery into eukaryotic cells (Birtalan *et al.*, 2002). It should be noted that these need not be mutually exclusive functions.

Type III secretion chaperones bind their cognate effectors in the vicinity of their N-termini, immediately adjacent to the primary secretion signals (Wattiau & Cornelis, 1993; Wattiau *et al.*, 1994; Cheng *et al.*, 1997). The structures of five type III secretion chaperones have been determined to date: *Y. pestis* SycE (Birtalan & Ghosh, 2001; Evdokimov *et al.*, 2002), enteropathogenic *Escherichia coli* CesT (Luo *et al.*, 2001), *Salmonella enterica* SicP (Stebbins & Galan, 2001) and SigE (Luo *et al.*, 2001) and *Shigella flexneri* Spa15 (Van Eerde *et al.*, 2004). Despite the fact that their amino-acid sequences are not conserved, all of these proteins adopt similar folds. They are homodimers, with each monomer consisting of three α-helices and a five-stranded antiparallel β-sheet.

SicP and SycE have been crystallized in complex with the chaperone-binding domains (CBDs) of their cognate effectors SptP and YopE, respectively (Stebbins & Galan, 2001; Birtalan *et al.*, 2002). The CBDs wrap around the homodimeric chaperones in an extended horseshoe-like conformation with some secondary structure but little or no tertiary structure. Because they are poorly soluble and/or readily degraded by proteases, these authors concluded that the CBDs of YopE and SptP are probably disordered in the absence of their cognate chaperones (Stebbins & Galan, 2001; Birtalan *et al.*, 2002). By contrast, the CBD of the protein tyrosine phosphatase (PTPase) YopH is a stably folded globular domain (Evdokimov *et al.*, 2001). Hence, if SycH binds YopH in the same manner that SicP and SycE interact with the CBDs of their cognate effectors, then it would have to do so by unfolding the N-terminal domain of YopH.

The amino-acid sequences of two other secreted *Yersinia* proteins, YscM1 and YscM2, resemble that of the YopH CBD (Evdokimov *et al.*, 2001). All pathogenic species of *Yersinia* produce YscM1, whereas YscM2 is confined to *Y. enterocolitica* (Stainier *et al.*, 1997). The YscM proteins are thought to function as a global regulators of type III secretion that repress the expression of virulence genes prior to contact with eukaryotic cells (Cambronne & Schneewind, 2002; Cambronne *et al.*, 2004). The high degree of sequence similarity between YscM1, YscM2 and the CBD of YopH suggests that all three proteins are likely to adopt similar folds. Here, we report the crystal structure of *Y. pestis* SycH in complex with residues 33–81 of YscM2. The structure is consistent with the hypothesis that SycH binds to an unfolded form of YscM2, implying that similar conformational changes also take place upon binding of SycH to YscM1 and the CBD of YopH.

2. Materials and methods

2.1. Construction of the SycH(1–138)/YscM2(33–81)-His$_6$ expression vectors

The vector used to coexpress residues 1–138 of SycH with residues 33–81 of YscM2 was constructed by Gateway multisite recombinational cloning (Invitrogen). The first open reading frame (ORF) in the bicistronic mRNA encoded residues 33–81 of YscM2. A His$_6$ tag was added to the C-terminus of this ORF during PCR amplification. The second ORF encoded residues 1–138 of SycH. A ribosome-binding site was added in the appropriate position upstream of this ORF during PCR amplification. The L8M mutant of SycH was constructed by altering the sequence of the PCR primer that was designed to anneal to the N-terminal end of the SycH ORF. The YscM2(33–81)-His$_6$ and SycH(1–138) PCR products were inserted by recombinational cloning into the donor vectors pDONR208 and pDONR209, respectively (Invitrogen). After the nucleotide sequences of the ORFs had been confirmed experimentally, they were moved by recombinational cloning into the destination vector pDEST-42 (Invitrogen) to create the bicistronic T7 expression vectors.

2.2. Protein expression and purification

The YscM2(33–81)-His$_6$–SycH(1–138) complex was overproduced in *E. coli* BL21(DE3) CodonPlus-RIL cells (Stratagene). Single antibiotic-resistant colonies were used to inoculate 100 ml Luria broth (Miller, 1972) supplemented with 100 μg ml^{-1} ampicillin and 30 μg ml^{-1} chloramphenicol. These cultures were grown with shaking (225 rev min^{-1}) to saturation overnight at 310 K and then diluted 66-fold into several litres of fresh medium. When the cells reached early log phase ($OD_{600\,nm}$ = 0.3–0.5), the temperature was reduced to 303 K and isopropyl β-D-thiogalactopyranoside (IPTG) was added to a final concentration of 1 m*M*. 4 h later, the cells were recovered by centrifugation at 5000*g* for 10 min and stored at 193 K.

E. coli cell paste was suspended in ice-cold 50 m*M* sodium phosphate pH 7.5, 200 m*M* NaCl, 25 m*M* imidazole (buffer *A*) containing Complete EDTA-free protease-inhibitor cocktail (Roche Molecular Biochemicals) and 1 m*M* benzamidine. The cells were lysed with an APV Gaulin Model G1000 homogenizer at 69 MPa and centrifuged at 30 000*g* for 30 min at 277 K. The supernatant was filtered through a 0.2 μm polyethersulfone membrane and applied onto a 30 ml Ni–NTA Superflow affinity column (Qiagen) equilibrated in buffer *A*. The column was washed with five column volumes of equilibration buffer and eluted with a linear gradient from 25 to 250 m*M* imidazole. Fractions containing recombinant SycH(1–138)–YscM2(33–81)-His$_6$ complex were pooled and dithiothreitol (DTT) was added to a final concentration of 5 m*M*. The sample was concentrated using an Amicon YM3

membrane (Millipore) and applied onto a 26/60 HiLoad Superdex 75 prep-grade column (Amersham Biosciences) equilibrated with 25 m*M* Tris pH 7.2, 150 m*M* NaCl, 2 m*M* DTT. The peak fractions containing the SycH(1–138)–YscM2(33–81)-His_6 complex were pooled and concentrated to 20–25 mg ml^{-1}. Aliquots were flash-frozen with liquid nitrogen and stored at 193 K until use. The final product was judged to be >95% pure by SDS–PAGE (data not shown). The molecular weights were confirmed by electrospray mass spectrometry (ESMS), which revealed some heterogeneity at the N-terminus of YscM2(33–81) arising from the incomplete removal of the initiator methionine by methionine aminopeptidase *in vivo*. The selenomethionine (SeMet) substituted SycH(1–138)–YscM2(33–81)-His_6 complexes (with either wild-type SycH or the L8M mutant) were produced using the saturation of the methionine-biosynthetic pathway protocol (Doublié, 1997) and purified in the same manner as the unlabeled protein complex; ESMS indicated that selenomethionine substitution was >99%.

2.3. Crystallization

The initial crystals of the SycH(1–138)–YscM2(33–81)-His_6 complex (15–30 mg ml^{-1} in 25 m*M* Tris pH 7.2, 150 m*M* NaCl and 2 m*M* DTT) were obtained from the Wizard I sparse-matrix crystallization screen (Emerald Biosciences) using the vapor-phase diffusion hanging-drop technique at 291 K. One drop with a thick film and oil also contained extremely fine microcrystals clinging to the surface of the cover slide (Fig. 1*a*). The conditions were 2 *M* $(NH_4)_2SO_4$, 100 m*M* CAPS pH 10.5 and 200 m*M* Li_2SO_4 (solution No. 33). It was difficult to get the crystals to grow larger and not adhere to the surface of the cover slide. Microseeding resulted in either a heavy shower of oil or a sheet of crystals, despite pre-equilibration time and precipitant concentration adjustments (Fig. 1*b*). Only after much effort had been invested did we finally obtain single crystals that were suitable for data collection (Fig. 1*c*). The optimized conditions consisted of 1.8 *M* $(NH_4)_2SO_4$, 100 m*M* CAPSO pH 9.6, 200 m*M* magnesium formate, 2% dioxane and 1.6 m*M* CHAPS. The optimum ratio of protein to precipitant was 1:4 µl and before the well was sealed, 0.4 ml of paraffin oil was added on top of the precipitant (1 ml) in the reservoir to control the evaporation rate. Within 24 h, single hexagonal crystals appeared and continued to grow to final dimensions of 0.5 × 0.5 × 0.8 mm after 42 h. The SeMet-substituted wild-type and L8M SycH(1–138)–YscM2(33–81)-His_6 complexes were crystallized similarly, except that the protein concentration was 60 mg ml^{-1} and the drop ratio was 1:3 µl.

2.4. X-ray data collection

Cryogenic protection proved to be a challenge for these crystals. Conventional protectants such as glycerol, glycols, alcohols, organic salts, sugars and Paratone-N either failed to adequately prevent crystals from cracking or yielded a highly smeared diffraction pattern. In retrospect, we believe that this may have been because of the fact that the molecules pack on their edges in a manner that creates large solvent channels in the crystal lattice. Eventually, mineral oil was successfully utilized to protect the crystals for low-temperature data collection. Medium-sized crystals were fished out of the drop with a nylon loop, dragged gently across the cover slide to remove excess mother liquor, immersed in mineral oil and then flash-cooled with liquid nitrogen for data collection at the SER-CAT insertion-device beamline 22-ID (Advanced Photon Source, Argonne National Laboratory). The data were reduced with the *HKL*2000 suite of programs (Otwinowski & Minor, 1997). The SycH(1–138)–YscM2(33–81)-His_6 complex crystallized in the $P6_122$ space group with one SycH–YscM2 heterodimer in the asymmetric unit. The crystals had a specific volume (V_M) of 2.20 $Å^3$ Da^{-1} and 42.8% solvent content. The unit-cell parameters were $a = b = 64.04$, $c = 161.20$ Å.

3. Results

3.1. Preparation of SycH–YopH, SycH–YscM1 and SycH–YscM2 complexes

SycH is the cognate secretion chaperone for the *Yersinia* effector YopH, a potent eukaryotic-like PTPase (Wattiau *et al.*, 1994; Bliska *et al.*, 1991). Like the other type III secretion chaperones, SycH binds to a site near the N-terminus of its cognate effector. However, the N-terminus of YopH adopts a

(*a*) (*b*) (*c*)

Figure 1
Crystals of the SycH(1–138)–YscM2(33–81)-His_6 complex. (*a*) Initial conditions showing an oily drop with extremely fine microcrystals. (*b*) Improved amorphous crystals. (*c*) Optimized diffraction-quality crystals.

well ordered compactly folded structure in the absence of SycH (Evdokimov *et al.*, 2001), whereas the N-terminus of YopE appears to be disordered in the absence of SycE (Birtalan *et al.*, 2002). If SycH binds YopH in the same manner that SycE interacts with YopE (Birtalan *et al.*, 2002), then the chaperone would have to unfold the N-terminal domain of YopH into an extended conformation. To determine whether this is indeed the case, we first attempted to crystallize a complex between SycH and the N-terminal domain of YopH (residues 1–130) (Evdokimov *et al.*, 2001) that was assembled by mixing the individually purified polypeptides together and then isolating the complex by gel-filtration chromatography. The resulting SycH–YopH(1–130) complex proved to be recalcitrant to crystallization. Therefore, we subjected it to limited proteolysis with thermolysin.

Consistent with the idea that the conformation of YopH may be significantly different in the presence or absence of SycH, we found that the YopH polypeptide was degraded much more rapidly and extensively by thermolysin when it was bound to SycH than when it was not (data not shown). Nevertheless, we were able to identify a prominent metastable digestion product of YopH that appeared to be protected by SycH. On the basis of mass spectrometry and N-terminal amino-acid sequencing data, we could confidently conclude that this fragment corresponds to residues 31–92 of YopH. The endpoints of this fragment were in fairly good agreement with the boundaries of the SycH-binding site defined by deletion mutagenesis (Sory *et al.*, 1995) and it is similar in length to the fragment of YopE that is bound by SycE (Birtalan *et al.*, 2002). The three C-terminal residues of SycH (139–141) were also efficiently removed by thermolysin in this experiment. Therefore, all SycH expression vectors were subsequently designed to produce residues 1–138.

SycH also binds to YscM1 and YscM2, which are negative regulators of type III secretion in *Yersinia* (Stainier *et al.*, 1997; Cambronne *et al.*, 2000; Wulff-Strobel *et al.*, 2002; Cambronne & Schneewind, 2002). The amino-acid sequences of YscM1 and YscM2 are similar to that of the N-terminal CBD of YopH (42 and 32% identity, respectively; Evdokimov *et al.*, 2001). Thus, SycH is likely to interact with all three of these proteins in an analogous manner. Unfortunately, although we had no difficulty reconstituting stable SycH–YscM1 and SycH–YscM2 complexes from individually purified polypeptides, we were unable to grow crystals of either of them. Therefore, at the same time that we constructed a vector to coexpress the thermolysin-resistant fragment of YopH (residues 31–92) with SycH (residues 1–138), we also constructed analogous vectors to coexpress the corresponding fragments of YscM1 (residues 29–78) and YscM2 (residues 33–81) with SycH(1–138). In all three cases, the polypeptides formed stable complexes that could be purified to homogeneity.

Table 1
Crystallographic data, phasing and refinement statistics.

Values in parentheses are for the last shell.

Data set	Native	SeMet	SeMet (L8M)	Deriv. 1†	Deriv. 2‡
Wavelength (Å)	0.9793	0.9794	0.9793	1.039	1.039
Resolution (Å)	25.0–2.38	25.0–2.5	25.0–2.5	25.0–2.7	25.0–2.6
Unique reflections	9196	7302	11663	5782	6572
Completeness (%)	98.7	98.6	92.2	97.6	99.1
Redundancy	13.1	20.1	10.2	13.7	13.2
Mosaicity (°)	0.90	0.21	0.37	0.55	0.37
$I/\sigma(I)$	26.9 (4.1)	32.6 (10.5)	19.0 (3.9)	24.9 (6.3)	29.1 (5.8)
$R_{\rm merge}$ (%)	6.9 (45.0)	7.2 (29.0)	8.3 (32.0)	7.2 (40.0)	6.9 (42.0)
No. sites		1	2	1	1
Anomalous differences (%)		4.6	9.1		
Isomorphous differences (%)				15.4	12.5
Phasing power					
Anomalous		1.0	0.67		
Isomorphous (centric/acentric)				0.96/1.1	0.77/0.90
Figure of merit (20–2.5 Å)					
Phasing		0.51			
After density modification		0.63			
Refinement resolution (Å)		25–2.38			
$R_{\rm cryst}$ (%)		24.3			
$R_{\rm free}$ (%)		29.2			
Average B factors (Å^2)		68.7			
R.m.s.d. bonds (Å)		0.04			
R.m.s.d. angles (°)		3.5			
No. molecules in AU					
Peptide		2			
Water		45			
Ramachandran analysis (%)					
Most favored		73.6			
Allowed		26.4			

† Wild-type SeMet protein cocrystallized with 0.1 m*M* trimethyllead acetate. ‡ Wild-type SeMet crystal soaked with 1.0 m*M* trimethyllead acetate overnight.

3.2. Crystallization of the SycH(1–138)–YscM2(33–81)-His$_6$ complex

Although all three protein complexes exhibited some propensity to crystallize (*i.e.* they readily formed organized precipitates), only the SycH(1–138)–YscM2(33–81)-His$_6$ complex yielded crystals with sharply defined edges (Fig. 1*c*). These crystals diffracted X-rays to 2.4 Å resolution, allowing a complete native data set to be collected.

Unfortunately, efforts to obtain derivatives by soaking or cocrystallization with heavy atoms were unsuccessful. This may have been in part a consequence of the high ammonium sulfate content and the alkaline pH (10.5) at which the protein complex crystallized. Efforts to solve the structure by molecular replacement using the coordinates of SycE as a search model also failed. Therefore, we next prepared a sample of SeMet-labeled SycH(1–138)–YscM2(33–81)-His$_6$ complex for a multiple anomalous dispersion (MAD) experiment. There are a total of four methionine residues in the complex,

including one at the N-terminus of each polypeptide. Curiously, even though mass spectrometry indicated that the Se atoms were clearly present and a strong anomalous signal was detected by a fluorescence scan, the structure could not be solved by the MAD or SAD methods.

Thinking that perhaps the methionine residues were disordered in the crystal, we decided to introduce an additional methionine residue into SycH by site-directed mutagenesis. We reasoned that if the structure of SycH resembles that of SycE and the other type III secretion chaperones, then Leu8 should be situated on the buried side of the N-terminal α-helix. Leu is considered the closest isosteric replacement for Met and Leu-to-Met substitutions occur frequently in orthologous proteins (Gassner & Matthews, 1999). Fortunately, the L8M mutation did not affect the yield or solubility of SycH(1–138), nor did it interfere with the formation of a stable complex between SycH(1–138) and YscM2(33–81)-His_6. Both wild-type and mutant SeMet-labeled SycH(1–138)–YscM2(33–81)-His_6 complexes crystallized under the same conditions as the native protein, except the protein concentration had to be raised to 60 mg ml^{-1} to produce diffraction-quality crystals. Interestingly, crystals of the SeMet-substituted complexes exhibited much lower mosaicity than those of the native protein.

3.3. Data collection, structure solution and refinement

MAD data were collected from crystals of complexes between YscM2(33–81)-His_6 and both the wild-type and L8M forms of SycH(1–138) and were processed with the *HKL*2000 suite of programs (Otwinowski & Minor, 1997). Unexpectedly, the structure could not be solved by the MAD technique owing to non-isomorphism resulting from crystal decay during the course of data collection and disorder of the methionine residues. Of the four methinonines present, only Met52 of SycH was ordered in the structure. Ironically, this Met becomes partially disordered in the L8M structure and thus does not yield sufficient information for MAD phasing of the L8M data. However, when the peak data from the wild-type and L8M crystals were combined with two other data sets obtained by cocrystallization of the SeMet-labeled wild-type complex with 0.1 m*M* trimethyllead acetate (TMLA) and overnight soaking with 1 m*M* TMLA (Deriv. 1 and Deriv. 2, respectively, in Table 1), the resulting phases yielded a clearly interpretable electron-density map (Fig. 2). The native data set, the peak-wavelength data from the wild-type SeMet and the L8M SeMet derivatives and the data obtained from Deriv. 1 and Deriv. 2 were combined into a pseudo-MIRAS script to run in the automated phasing package *SOLVE* (Terwilliger & Berendzen, 1999). The keyword 'ano only' was applied to anomalous peak data and 'iso only' to Deriv. 1 and Deriv. 2. Although no Pb atom was located in the Patterson map after soaking or cocrystallization, the latter data sets contained the SeMet-substituted residues, which provided strong isomorphous differences for phasing (Table 1). They both showed a 20σ peak at the position of Met52. In addition, a similar peak was observed for the L8M mutant at the relative position of Leu8, affirming the rationale for choosing this mutation.

The phased data from *SOLVE* was subjected to statistical density modification with prime-and-switch minimal-bias phasing, motif recognition and automatic model building using its sister program *RESOLVE* (Terwilliger & Berendzen, 1999). With a solvent content of 45%, the figure of merit could be improved by more than 10% by density modification (Table 1).

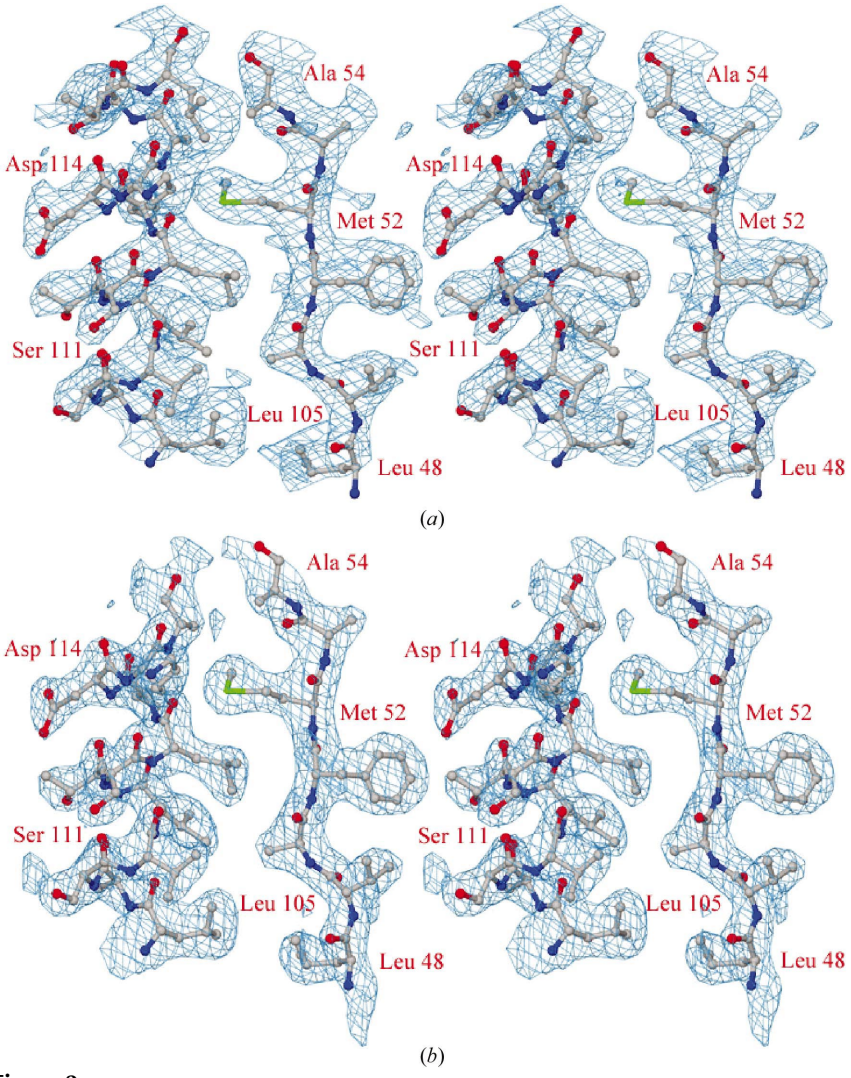

Figure 2
A sample of the MIRAS-phased map superimposed on the final model (*a*) and the refined map (*b*), both contoured at 1.2σ. Graphics were produced by *O* and rendered with *MOLRAY* (Harris & Jones, 2001).

A good portion of the map was traced automatically, with 40% of the residues having their side chains placed correctly. The partial model was manually adjusted and extended with the graphics program *O* (Jones *et al.*, 1991) and then refined with *REFMAC*5 (Murshudov *et al.*, 1997) (Table 1). The final model included residues 3–120 of SycH and 33–50 of YscM2. Despite the high temperature factors, the structure of SycH was quite well resolved. However, side chains could only be assigned to the helical portion of YscM2. The remainder of this polypeptide was poorly ordered in the crystal. Only side-chain density for C^{β} atoms was observed and so these residues were modeled as alanines.

3.4. Description of the structure

3.4.1. SycH. As anticipated, the structure of SycH is very similar to those of the other TTSS chaperones. A three-dimensional structural search with the DALI server (Holm & Sander, 1994) yielded a number of statistically significant hits, including SycE (*Z* score 14.3 and r.m.s.d. 2.3 Å), SicP (12 and 2.6 Å), Spa15 (10.7 and 3.2 Å) and SigE (9.2 and 3.1 Å), all of which share very little sequence similarity with SycH or each other. The SycH monomer is comprised of a slightly twisted five-stranded antiparallel β-sheet leaning against a long α-helix on one side and flanked by two shorter α-helices near its edges (Fig. 3*a*). Although the asymmetric unit of the crystal contains only one molecule of SycH, the biologically relevant form of the protein is expected to be a homodimer (Parsot *et al.*, 2003). Indeed, two symmetry-related molecules in the crystal lattice form an extensive interface that buries approximately 1100 $Å^2$ per monomer (*CNS*; Brünger *et al.*, 1998) and resembles those observed in the structures of other type III secretion chaperones (Fig. 3). The C-terminus of SycH (after residue 120) is disordered in the crystal.

3.4.2. YscM2. Residues 51–81 of the YscM2(33–81) polypeptide are disordered in the crystal and only the side chains in the α-helical segment could be assigned with confidence. Nevertheless, it is clear that the interaction of the N-terminal part of YscM2 (residues 33–50) with SycH closely resembles the manner in which the N-terminus of YopE binds to SycE, the nearest structural relative of SycH (Fig. 4). As observed in the structure of the SycE–YopE CBD complex (Birtalan *et al.*, 2002), the N-terminus of the CBD (YscM2 in this case) engages in an intermolecular β-strand interaction with β-1 of the chaperone (SycH in this case), augmenting the edge of the

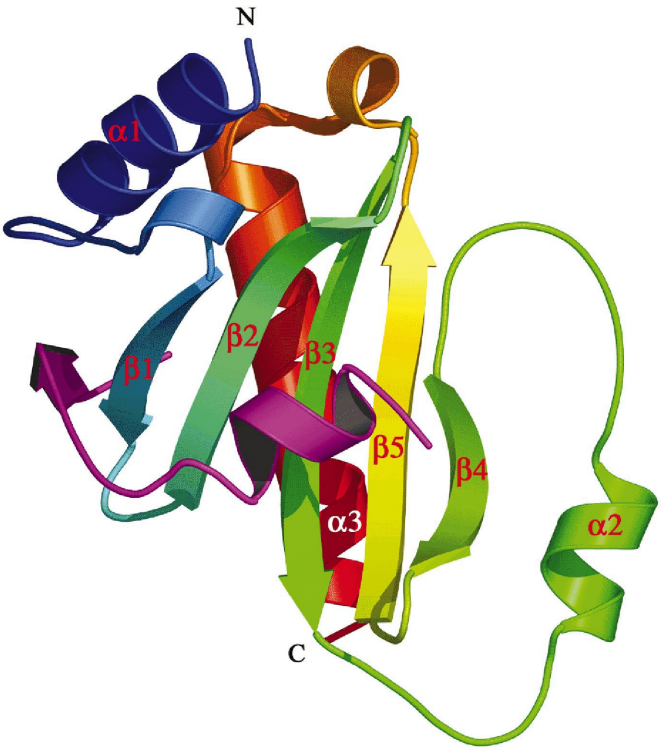

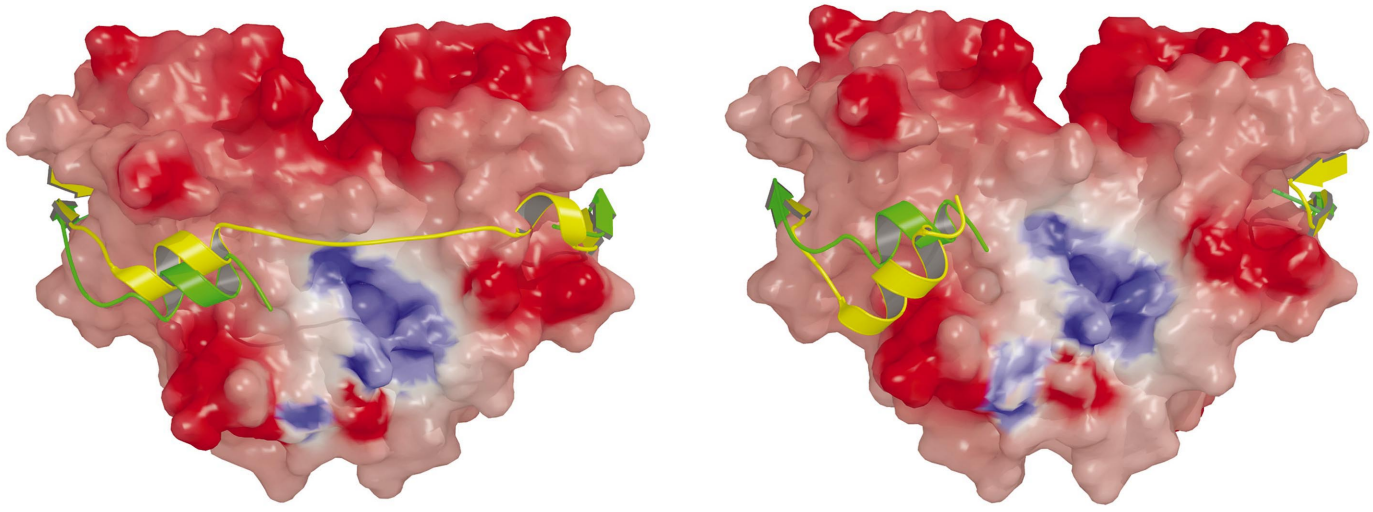

(*b*)

Figure 3
(*a*) Ribbon representations of monomeric SycH (rainbow coloring) in complex with a fragment of YscM2 (in magenta). (*b*) Molecular-surface diagrams of SycH with YscM2 depicted as a green ribbon and the superimposed YopE from the SycE–YopE complex in yellow: front view (left) and back view (right). Graphics were generated with *MOLSCRIPT* (Kraulis, 1991), *RASTER3D* (Merritt & Murphy, 1994) and *GRASP* (Nicholls *et al.*, 1991).

β-sheet. The YscM2 polypeptide then wraps around the edge of the chaperone in an extended conformation until it reaches a conserved hydrophobic patch on the surface of SycH that is analogous to 'patch 1' on SycE (Birtalan *et al.*, 2002). Here, YscM2 takes on an α-helical configuration, just as YopE does when it interacts with patch 1 on SycE. Beyond this point, the YscM2 polypeptide becomes disordered. In the structure of the SycE–YopE CBD complex, the CBD of YopE reaches from patch 1 all the way around the surface of the chaperone to the back of the other subunit where it interacts with 'patch 2', the symmetric equivalent of patch 1 (Fig. 3*b*). In retrospect, we now believe that we may have been misled by the results of the limited proteolysis experiments on the YopH(1–130)–SycH complex and inadvertently selected a fragment of YscM2 that is too short to reach around the chaperone and interact with patch 2. Indeed, we noticed that the truncated YscM2 polypeptide did not bind as tightly to SycH as did full-length YscM2 during purification. This may explain why the asymmetric unit in the crystal is composed of one SycH–YscM2 heterodimer instead of a dimeric chaperone bound asymmetrically to one molecule of YscM2. Because the C-terminus of YscM2 was not available to interact with patch 2 on SycH, we may instead have crystallized a symmetric 2:2 complex with the N-terminal regions of two different YscM2 polypeptides bound to patch 1 and patch 2 of the homodimeric chaperone.

3.4.3. Conserved features of SycH and SycE that may be involved in secretion targeting. SycH is the second type III secretion chaperone from *Y. pestis* for which structural information has become available. Although the folds of the two chaperones are fundamentally similar, there are many subtle differences. These occur mainly in the loop and turn regions (α1–β1, β3–α2, α2–β4, β4–β5 and β5–α3) and at the dimer interfaces (Fig. 5). The turn from the β4–β5 hairpin in SycE is puckered away from the molecule and is extended in SycH. The shorter interface helices α2 cross each other at an angle in SycH compared with their slightly longer and parallel counterparts in SycE and the lasso that follows is longer and wider in SycH than in SycE (Fig. 4*a*). This α2–β4 loop is more planar in SycH and more curved in SycE (Fig. 4*b*). As a result, the contours of the dimer interfaces are significantly different in the two molecules.

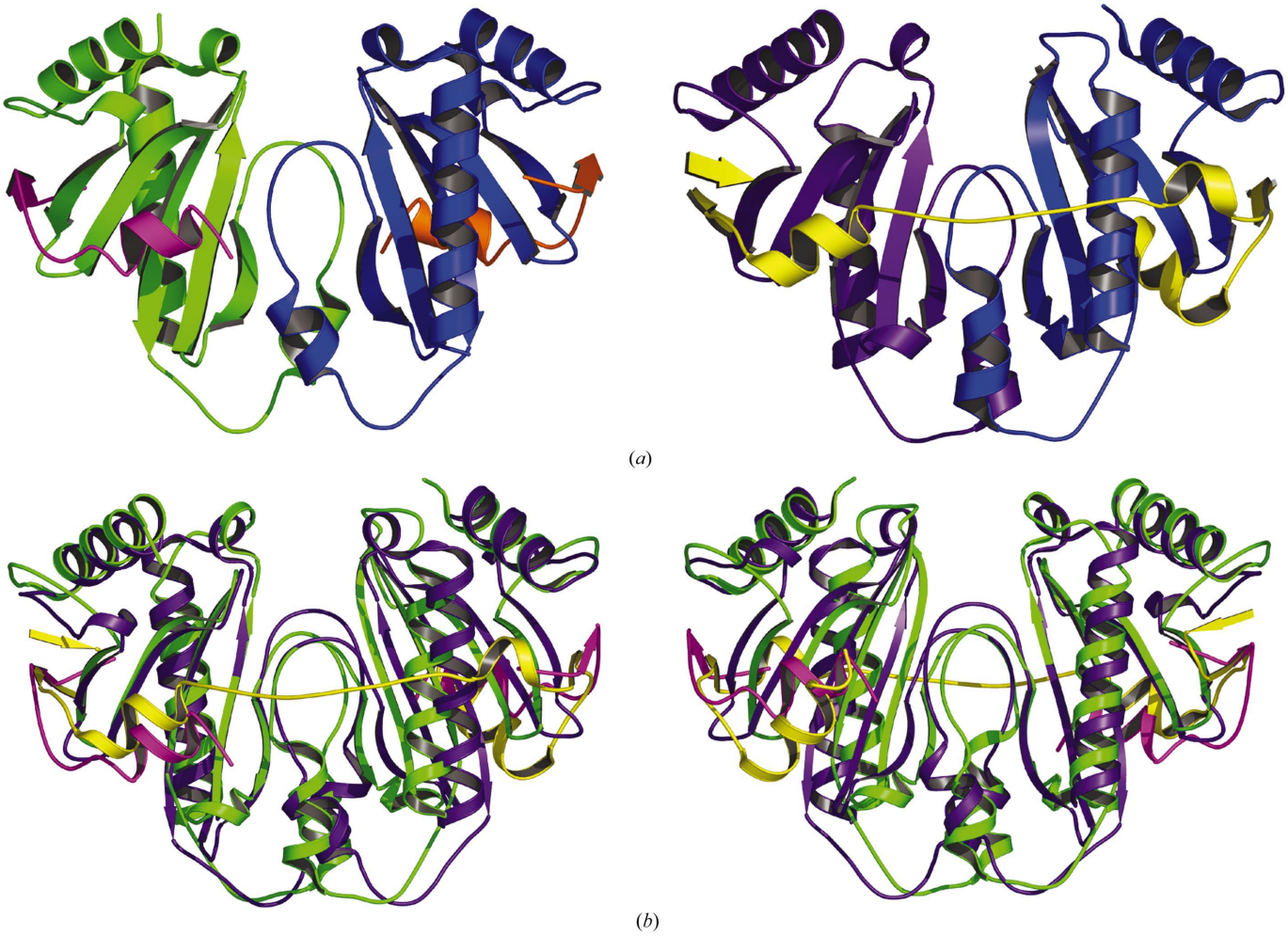

Figure 4
(*a*) Ribbon models of the SycH–YscM2 complex (left) and SycE–YopE complex (right). (*b*) Structural alignment of SycH–YscM2 in green and magenta and SycE–YopE in purple and yellow: front view (left) and back view (right). Graphics were generated with *MOLSCRIPT*, *RASTER3D* and *PyMOL* (DeLano Scientific).

The molecular surfaces of the two chaperones also differ in their detail, which is not surprising in light of the fact that their amino-acid sequences are not conserved. Both molecules are acidic overall, but the local distribution of electrostatic potential is generally not conserved. There is one exception, however. Both chaperones have a pair of symmetry-related positively charged residues (Arg80 in SycH and Arg92 in SycE) that are located inside substantial cavities of similar volume (~290 Å^3 in SycH and ~200 Å^3 in SycE) at the dimer interface (Fig. 6). We note that Arg92 is conserved in SpcS, the *P. aeruginosa* ortholog of SycE (Evdokimov *et al.*, 2002). Moreover, both the cavity and a pair of structurally equivalent positively charged residues are also conserved in the structures of CesT and SigE (Luo *et al.*, 2001) and in that of the heterodimeric secretion chaperone SycN–YscB, which has a similar fold (Schubot *et al.*, unpublished observations). Since this part of the chaperone does not interact with the CBD, we propose that it may serve to facilitate type III secretion by physically interacting with some component of the membrane-spanning secretion apparatus to initiate the process. The notion that TTSS chaperones may function in part as auxiliary secretion signals is not new (Birtalan *et al.*, 2002). However, thus far there has been only one instance in which experimental evidence for a direct interaction between a chaperone and some component of the TTSS apparatus has been obtained. In this case, the chaperone CesT was shown to interact with the membrane-associated TTSS ATPase EscN (Gauthier & Finlay, 2003). Whether or not this interaction involves the positively charged cavity at the dimer interface of CesT remains to be determined. However, the broad conservation of this feature in type III secretion chaperones, which does not appear to have a structural explanation, is certainly suggestive and merits further investigation.

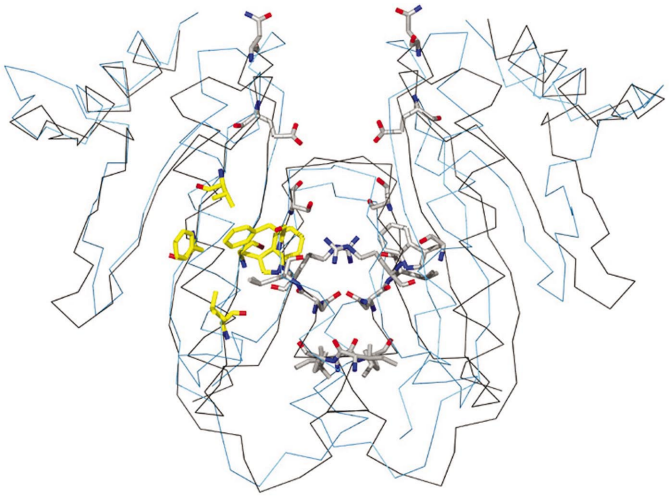

Figure 5
C^{α} alignment of SycH (gray) and SycE (sky blue) homodimers with residues from SycH that form a cavity at the dimer interface depicted with gray bonds (Glu47, Val49, Phe51, Ile66, Leu67, Asn70, Ile71, Phe72, Ser73, Arg80, Trp92 and Asn98) and conserved hydrophobic patch 1 residues (Val49, Phe51, Phe72, Leu90 and Trp 92) shown with yellow bonds.

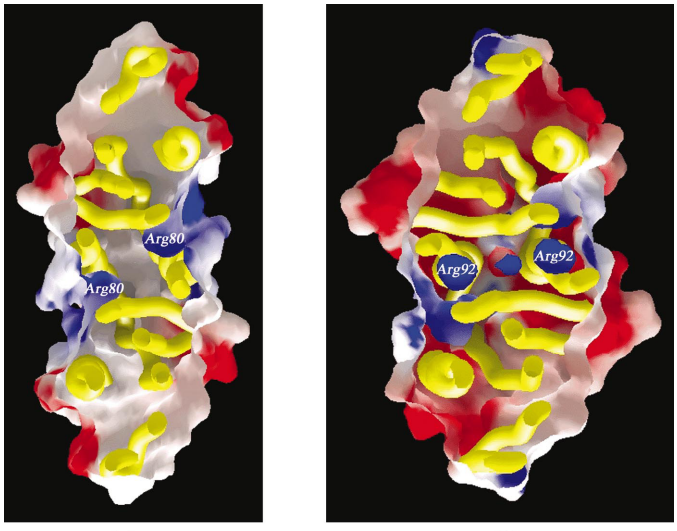

(*a*) (*b*)

Figure 6
Top view of a cross-section of the molecular surface and worm of SycH (*a*) and SycE (*b*) dimers showing electrostatic potentials inside the cavity. The highly conserved arginines that contribute to the positive potentials inside the cavities are labeled.

4. Discussion

The structure of SycH in complex with a fragment of YscM2 reveals a homodimeric chaperone with a fold that closely resembles those of the other type III secretion chaperones that have been determined to date. Although much of the YscM2 fragment is disordered in the crystal, its N-terminus follows a path along the surface of the chaperone that is very similar to that taken by the CBD of YopE on the surface of SycE (Figs. 3 and 4). Moreover, the conformation adopted by residues 33–50 of YscM2 is very similar to that of the analogous segment of YopE in the structure of the SycE–YopE CBD complex (Fig. 4*b*), although their amino-acid sequences are unrelated.

The N-terminus of YopM is disordered in the crystal structure (Evdokimov *et al.*, 2001) and the N-termini of several other effectors have been demonstrated to be quite labile to proteolysis (Stebbins & Galan, 2001; Birtalan *et al.*, 2002; Derewenda *et al.*, 2004), suggesting that they too may be disordered. Hence, YopH appears to be unique among the effectors that have been characterized thus far in that its N-terminus folds into a compact globular domain. Indeed, this globular domain plays a role in the recognition of substrates for tyrosine dephosphorylation in eukaryotic cells (Black *et al.*, 1998). Because considerable sequence similarity exists between the N-terminal CBD of YopH, YscM1 and YscM2, it is highly likely that all three of these proteins adopt similar structures. If so, then in order for any of them to present a disordered N-terminal secretion signal to the TTSS (*i.e.* a primary secretion signal) they would have to be unfolded to some extent. We propose that this is one important function of SycH, although, as discussed above, type III secretion chaperones may also play a role in secretion targeting.

Unfortunately, only part of the YscM2 fragment in the present structure was observed to interact with SycH.

However, it is enough to conclude on the basis of an amino-acid sequence alignment with the CBD of YopH (Evdokimov *et al.*, 2001) that its conformation is 'unwound' in the complex with SycH relative to its presumed globular fold. Although it may be purely coincidental, it is interesting to note that the same elements of secondary structure that are predicted to occur, by analogy with YopH, in the globular structure of YscM2 are recapitulated in the structure of the SycH–YscM2 complex. The residues of YscM2 that engage in the intermolecular β-strand interaction with SycH and those that form the α-helix that binds to patch 1 correspond respectively to strand β-2 and helix α-2 in the predicted globular fold of YscM2 (Evdokimov *et al.*, 2001). Moreover, in a longer fragment of YscM2 that extended nearly to its C-terminus, the residues that correspond to strand β-4 and helix α-4 in the predicted globular fold of YscM2 would be in approximately the correct positions to form pseudo-symmetrical interactions with the other subunit of SycH.

We thank Karen Routzahn, Howard Peters and Scott Cherry for expert technical assistance. Electrospray mass-spectrometry experiments were conducted on the LC/ESMS instrument maintained by the Biophysics Resource in the Structural Biophysics Laboratory, Center for Cancer Research, National Cancer Institute at Frederick. X-ray diffraction data were collected at the Southeast Regional Collaborative Access Team (SER-CAT) 22-ID beamline at the Advanced Photon Source, Argonne National Laboratory. Supporting institutions may be found at http://www.ser-cat.org/members.html. Use of the Advanced Photon Source was supported by the US Department of Energy, Office of Science, Office of Basic Energy Sciences under Contract No. W-31-109-Eng-38.

References

Birtalan, S. C. & Ghosh, P. (2001). *Nature Struct. Biol.* **8**, 974–978.
Birtalan, S. C., Phillips, R. M. & Ghosh, P. (2002). *Mol. Cell*, **9**, 971–980.
Black, D. S., Montagna, L. G., Zitsmann, S. & Bliska, J. B. (1998). *Mol. Microbiol.* **29**, 1263–1274.
Bliska, J. B., Guan, K. L., Dixon, J. E. & Falkow, S. (1991). *Proc. Natl Acad. Sci. USA*, **88**, 1187–1191.
Boland, A., Sory, M. P., Iriarte, M., Kerbourch, C., Wattiau, P. & Cornelis, G. R. (1996). *EMBO J.* **15**, 5191–5201.
Brünger, A. T., Adams, P. D., Clore, G. M., DeLano, W. L., Gros, P., Grosse-Kunstleve, R. W., Jiang, J.-S., Kuszewski, J., Nilges, M., Pannu, N. S., Read, R. J., Rice, L. M., Simonson, T. & Warren, G. L. (1998). *Acta Cryst.* D**54**, 905–921.
Cambronne, E. D., Cheng, L. W. & Schneewind, O. (2000). *Mol. Microbiol.* **37**, 263–273.
Cambronne, E. D. & Schneewind, O. (2002). *J. Bacteriol.* **184**, 5880–5893.
Cambronne, E. D., Sorg, J. A. & Schneewind, O. (2004). *J. Bacteriol.* **186**, 829–841.
Cheng, L. W., Anderson, D. M. & Schneewind, O. (1997). *Mol. Microbiol.* **24**, 757–765.
Cornelis, G. R. (2002). *Nature Rev. Mol. Cell Biol.* **3**, 742–752.
Derewenda, U., Mateja, A., Devedjiev, Y., Routzahn, K. M., Evdokimov, A. G., Derewenda, Z. S. & Waugh, D. S. (2004). *Structure*, **12**, 301–306.
Doublié, S. (1997). *Methods Enzymol.* **276**, 523–530.
Evdokimov, A. G., Tropea, J. E., Routzahn, K. M., Copeland, T. D. & Waugh, D. S. (2001). *Acta Cryst.* D**57**, 793–799.
Evdokimov, A. G., Tropea, J. E., Routzahn, K. M. & Waugh, D. S. (2002). *Acta Cryst.* D**58**, 398–406.
Gassner, N. C. & Matthews, B. W. (1999). *Acta Cryst.* D**55**, 1967–1970.
Gauthier, A. & Finlay, B. B. (2003). *J. Bacteriol.* **185**, 6747–6755.
Harris, M. & Jones, T. A. (2001). *Acta Cryst.* D**57**, 1201–1203.
Holm, L. & Sander, C. (1994). *Proteins*, **19**, 165–173.
Jones, T. A., Zou, J. Y., Cowan, S. W. & Kjeldgaard, M. (1991). *Acta Cryst.* A**47**, 110–119.
Kraulis, P. J. (1991). *J. Appl. Cryst.* **24**, 946–950.
Lloyd, S. A., Sjostrom, M., Andersson, S. & Wolf-Watz, H. (2002). *Mol. Microbiol.* **43**, 51–59.
Luo, Y., Bertero, M. G., Frey, E. A., Pfuetzner, R. A., Wenk, M. R., Creagh, L., Marcus, S. L., Lim, D., Sicheri, F., Kay, C. & Strynadka, N. C. (2001). *Nature Struct. Biol.* **8**, 1031–1036.
Merritt, E. A. & Murphy, M. E. P. (1994). *Acta Cryst.* D**50**, 869–873.
Miller, J. H. (1972). *Experiments in Molecular Genetics*. New York: Cold Spring Harbor Press.
Murshudov, G. N., Vagin, A. A. & Dodson, E. J. (1997). *Acta Cryst.* D**53**, 240–255.
Nicholls, A., Sharp, K. & Honig, B. (1991). *Proteins*, **11**, 281–296.
Otwinowski, Z. & Minor, W. (1997). *Methods Enzymol.* **276**, 307–326.
Parsot, C., Hamiaux, C. & Page, A.-L. (2003). *Curr. Opin. Microbiol.* **6**, 7–14.
Ramamurthi, K. S. & Schneewind, O. (2003). *Mol. Microbiol.* **50**, 1095–1102.
Schesser, K., Frithz-Lindsten, E. & Wolf-Watz, H. (1996). *J. Bacteriol.* **178**, 7227–7233.
Sory, M. P., Boland, A., Lambermont, I. & Cornelis, G. R. (1995). *Proc. Natl Acad. Sci. USA*, **92**, 11998–12002.
Stainier, I., Iriarte, M. & Cornelis, G. R. (1997). *Mol. Microbiol.* **26**, 833–843.
Stebbins, C. E. & Galan, J. E. (2001). *Nature (London)*, **414**, 77–81.
Terwilliger, T. C. & Berendzen, J. (1999). *Acta Cryst.* D**55**, 849–861.
Trulzsch, K., Roggenkamp, A., Aepfelbacher, M., Wilharm, G., Ruckdeschel, K. & Heesemann, J. (2003). *Int. J. Med. Microbiol.* **293**, 167–177.
Van Eerde, A., Hamiaux, C., Perez, J., Parsot, C. & Dijkstra, B. W. (2004). *EMBO Rep.* **5**, 477–483.
Wattiau, P., Bernier, B., Deslee, P., Michiels, T. & Cornelis, G. R. (1994). *Proc. Natl Acad. Sci. USA*, **91**, 10493–10497.
Wattiau, P. & Cornelis, G. R. (1993). *Mol. Microbiol.* **8**, 123–131.
Wattiau, P., Woestyn, S. & Cornelis, G. R. (1996). *Mol. Microbiol.* **20**, 255–262.
Wulff-Strobel, C. R., Williams, A. W. & Straley, S. C. (2002). *Mol. Microbiol.* **43**, 411–423.